doi: 10.1111/j.1460-2695.2005.00908.x

Crack trapping effect of persistent grain boundary islands

X. KONG and Y. QIAO

Department of Civil Engineering, University of Akron, Akron, OH 44325-3905, USA

Received in final form 3 February 2005

ABSTRACT In the polycrystalline Fe–Si alloy, when a cleavage front transmits from one grain to another, it first penetrates stably across the grain boundary at a number of breakthrough points (BTPs) that distribute along the front quasi-periodically. As the critical energy release rate is reached, unstable crack jump occurs and the persistent grain boundary islands (PGBI) between the BTPs are left behind the verge of propagating, bridging across the crack flanks, which leads to a 10–30% increase in fracture resistance. In this article, this process is investigated through an energy analysis. The influence of the size/spacing ratio of PGBI on the grain boundary toughness is discussed in detail.

Keywords crack trapping; fracture; grain boundaries; toughness.

INTRODUCTION

The important role of high-angle grain boundaries in fracture in intrinsically brittle metals and alloys has been widely noticed for many decades. As a cleavage crack front is usually arrested by an array of grain boundaries, the resistance to cracking is actually determined by the grain boundary toughness. A number of experimental observations indicate that the ductile-to-brittle transition temperature is a function of the grain structure,[1–3] which is sometimes attributed to the presence of grain boundary inclusions[4,5] and/or the boundary–dislocation interaction.[6,7] In the former framework, the cleavage cracking is related to the failure of one or a few large grain boundary imperfections, such as carbides, whereas in the latter, the grain boundary is considered as the barrier to dislocation transmission in the first grain and the source of dislocation emission in the second grain, which results in the deceleration–acceleration characteristic of the near-boundary crack advance. Although these studies have unquestionable utility in grain boundary engineering, they have shed little light on the structure dependence of the crack front behaviour, e.g. the geometrically necessary front branching.

A few early studies on the resistance of grain boundaries to cleavage cracking include the nitrogen-charged fracture experiment on Fe–3wt% Si polycrystals carried out by Gill and Smith,[8] in which the crystallographic misorientation of the two grains across a high-angle grain boundary was described by three microstructure factors accounting for the relative twist, tilt and rotation angles. The experimental results showed that the effect of the twist misorientation is more pronounced than that of the tilt misorientation, and the influence of the rotation misorientation is negligible. Such effects have been considered in a number of models of cleavage fracture in polycrystalline materials,[9–11] whereas the quantitative studies on the crack front–grain boundary interaction are rare.

In a recent experimental research on the grain boundary toughness of a set of Fe–3wt% Si bicrystals, the front transmission across high-angle grain boundaries and its influence on fracture resistance were analyzed in considerable detail.[12–15] When an advancing cleavage front encounters a grain boundary, it first transmits from the cleavage plane in the first grain ('A') to that of the second grain ('B') at a number of breakthrough points (BTP). The BTPs distribute along the boundary quasi-periodically. Near a BTP, the grain boundary separation occurs simultaneously as the front penetrates into grain 'B'. As the applied stress intensity increases, the front penetration depth keeps rising and, when the peak boundary resistance is reached, the cleavage front will bypass the boundary and jump forward. By accounting for the work of separation of cleavage facets in both the grain 'B' and the grain boundary, a simple expression has been projected for the boundary resistance[12]

$$\frac{G_0}{G_A} = \frac{\sin\theta + \cos\theta}{(\cos\psi)^2} + C\frac{\sin\theta\cos\theta}{\cos\psi},$$

where G_0 and G_A are the fracture resistances at the grain boundary and in the single crystal, respectively; θ and

Correspondence: Y. Qiao. E-mail: yqiao@uakron.edu

ψ are the twist and tilt misorientations, respectively, and $C = 0.25$ is a material constant. The factors of the shear strength of grain boundary and the average spacing between BTP come in by affecting C. However, although the result of this equation fits with the experimental data reasonably well, it is based on the assumption that the crack front advance is uniform, which is incompatible with the fractography study. In order to investigate the role of high-angle grain boundaries in cleavage cracking, the non-uniform nature of front propagation must be taken into consideration.

In the following sections, we will analyze the trapping effect of the grain boundary through an energy analysis. In this method, the simulation of the evolution of cleavage front profile, which can be prohibitively difficult due to the high aspect ratio and the nonlinear boundary–crack front interaction, is avoided.

CLEAVAGE CRACKING ACROSS A HIGH-ANGLE GRAIN BOUNDARY

As depicted in Fig. 1, the cleavage cracking across a high-angle grain boundary consists of the stable front penetration around the BTPs and the subsequent unstable crack jump. In order to calculate the critical energy release rate at the onset of unstable crack advance, consider the bicrystal double-cantilever-beam (DCB) specimen depicted in Fig. 2. The small bicrystal piece is attached to the polycrystalline carrier through perfect bonding, and initially the pre-crack tip is at the grain boundary. The details of the experimental procedure are given elsewhere.[12,13] With the quasi-static increase in crack opening displacement, the effective stress intensity at the crack tip rises, leading to the stable front transmission around the BTPs, where the grain boundary is separated through shear fracture. As

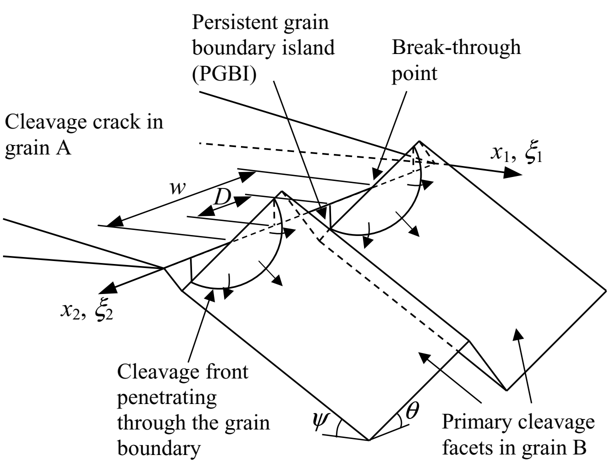

Fig. 1 A schematic diagram of the cleavage front transmitting across a high-angle grain boundary.

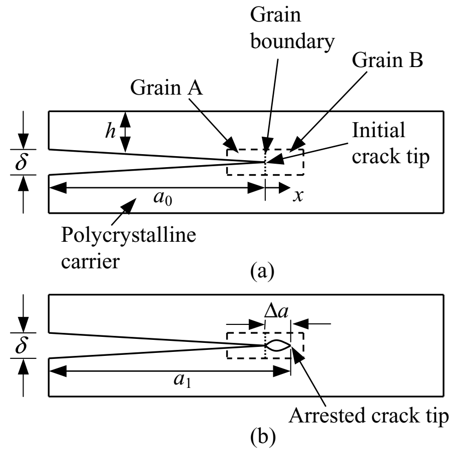

Fig. 2 A schematic diagram of the double-cantilever-beam specimen (a) prior to the crack jump and (b) after the crack jump.

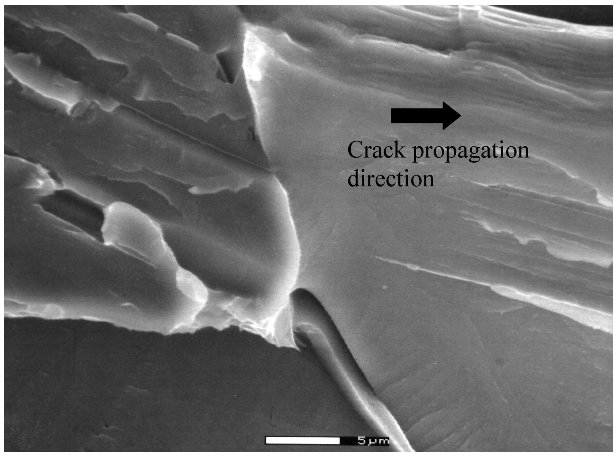

Fig. 3 SEM microscopy of a PGBI separated through plastic shear at $-25\ ^{\circ}$C in an Fe–3wt%Si bicrystal.

the penetration depth of the cleavage front is much smaller than the crack length, the variation in crack length can be neglected. When the energy release rate, G, reaches the critical value, G_{cr}, the cleavage front bypasses the array of the bridging boundary areas in between the BTPs, which will be referred to as persistent grain boundary islands (PGBI) in the following discussion, and jumps forward by a distance of Δa. The criterion of crack arrest can be stated as $G = G_{B0}$, with G_{B0} being the critical energy release rate to arrest the propagating crack in grain 'B'.

Figure 3 shows the SEM micrograph of a PGBI in an Fe–3wt%Si bicrystal that was separated after the fracture experiment had been finished. It can be seen clearly that the grain boundary was separated by shearing accompanied by significant plastic bending of the ligaments, indicating that the failure of PGBI is much more difficult than the cracking of crystallographic planes.[8,9] This observation is compatible with the model developed by

McClintock for the quasi-static fracture in polycrystals in which the mode of grain boundary separation was assumed to be pure shear combined with coplanar shear fracture.[11] The large extent of sigmodial bending of the ligaments connecting the cleavage facets at different levels demonstrates that the final separation of the PGBI cannot occur spontaneously before the cleavage front stops.

At the onset of the crack jump, through basic beam theory, we have

$$G_{\mathrm{cr}} = -\frac{1}{b}\frac{\partial U}{\partial a} = \frac{3}{16}\frac{Eh^3\delta^2}{a_0^4}, \tag{1}$$

where a_0 is the initial crack length, E and h are the modulus of elasticity and the height of DCB arm, respectively, U is the strain energy, a is the crack length, b is the sample thickness and δ is the crack opening displacement, which is a constant during the crack jump. Note that, because, as will become clear shortly, the sample geometry has little influence on G_{cr}, we can choose the ranges of h and a_0 such that the effects of the shear stresses, the strain energy in the background and the free edges are negligible.

Assume that there is a fracture resistance gradient in the material ahead of the initial crack tip such that the crack growth driving force, G, is always equal to the local fracture resistance, until the crack stops in grain 'B'. Under this condition, the crack advance is quasi-static and the criterion of crack stoppage can be stated as

$$G = G_{\mathrm{B}} = \frac{G_{\mathrm{A}}}{\cos\theta \cdot \cos\psi}, \tag{2}$$

where G_{B} is the fracture resistance of grain 'B'. As the fracture resistance gradient affects the crack tip behaviour only after the front bypasses the grain boundary, it has no influence on the value of G_{cr}.

If the PGBI could be separated before the crack front is arrested, similar to Eq. (1), we have $G_{\mathrm{B}} = 3Eh^3\delta^2/16a_1^4$, with $a_1 = a_0 + \Delta a$. If the grain boundary shear strength is large enough, the PGBI do not fail spontaneously and, due to the bridging effect, the effective energy release rate should be calculated through[16]

$$G_{\mathrm{B}} = \left(1-\nu^2\right)\bar{K}^2/E, \tag{3}$$

where

$$\bar{K} = \frac{1}{w}\int_0^w K(x_2)\mathrm{d}x_2 \tag{4}$$

and

$$K(x_2) = K_0 + \int_\Gamma H(s,\vec{\xi})P(\xi_2)\mathrm{d}\Gamma, \tag{5}$$

where ν is Poisson's ratio; w is the average distance between PGBI (see Fig. 1), $\vec{x} = (x_1, x_2)$ and $\vec{\xi} = (\xi_1, \xi_2)$ are the global and local coordinate systems in the crack plane, respectively, with the subscripts '1' denoting the crack propagation direction and '2' denoting the direction of the crack front line; K_0 is the stress intensity factor if the PGBI were separated; $s = |x_2 - \xi_2|$; Γ denotes the domain of PGBI; $P(\xi_2)$ is the bridging force distributed in PGBI, and $H(s,\vec{\xi}) = \sqrt{2/\pi^3}\cdot\sqrt{-\xi_1}/\left(s^2+\xi_1^2\right)$. Note that $K_0 = \sqrt{EG_0/(1-v^2)}$, where $G_0 = 3Eh^3\delta^2/16a_1^4$. Combination of Eqs (1) and (3) gives

$$\tilde{G} = \frac{3}{16(1-\nu^2)}\frac{E^2h^3\delta^2}{a_0^4\bar{K}^2}, \tag{6}$$

where $\tilde{G} = G_{\mathrm{cr}}/G_{\mathrm{B}}$.

The bridging force $P(\xi_2)$ should be obtained through the principal of compatibility. If $P(\xi_2) = 0$, the crack opening displacement at the PGBI is[16]

$$V(\vec{x}) = 2K_0\cdot\frac{1-\nu}{\mu}\sqrt{\frac{\Delta a}{2\pi}} \tag{7}$$

where μ is the shear modulus. Thus,

$$0 = V(\vec{x}_0) + \frac{1-\nu}{\mu}\int_\Gamma M(\vec{x}_0,\vec{\xi})P(\xi_2)\mathrm{d}\Gamma, \tag{8}$$

where $\vec{x}_0$ denotes any point in PGBI, $M(\vec{x},\vec{\xi}) = \frac{1}{\rho\pi^2}\times \arctan\left\{2\sqrt{\frac{x_1\xi_1}{\rho^2}}\right\}$ and ρ is the distance between $\vec{x}$ and $\vec{\xi}$.[17] Equation (8) is a Fredholm integral equation of the first kind, which can be solved numerically using the Ritz method. Note that the bridging force distribution in each PGBI is assumed to be identical and $K(x)$ is periodic.

Without the bridging PGBI, the strain energy change associated with the crack length increment Δa is

$$\Delta U_0 = \frac{a_0 b}{3}G_{\mathrm{cr}} - \frac{a_1 b}{3}G_{\mathrm{B}}. \tag{9}$$

Because of the additional strain energy caused by the bridging force $P(\xi_2)$, Eq. (9) should be modified as

$$\Delta U = \frac{a_0}{3}G_{\mathrm{cr}} - \frac{a_1}{3}G_{\mathrm{B}} - \frac{1}{w}\int_\Gamma P(\xi_2)V(\vec{\xi})\mathrm{d}\Gamma, \tag{10}$$

where ΔU is the change in strain energy per unit thickness, which, according to the energy equilibrium, must equal the fracture work

$$\Delta U = \int_0^{\Delta a} R(x)\mathrm{d}x, \tag{11}$$

where $R(x)$ is the local fracture resistance, and x denotes a point between the initial crack tip and the arrested crack front. As x increases from 0 to Δa, R decreases from G_{cr} to G_{B}. Similar to the discussion of Eq. (4), R consists of the contributions from both the remote loading and the bridging force, i.e.

$$R(x) = \left(1 - \nu^2\right) \tilde{K}(x)^2 / E, \tag{12}$$

where

$$\tilde{K}(x) = \frac{1}{w} \int_0^w \hat{K}(x, x_2) \mathrm{d}x_2 \tag{13}$$

and

$$\widehat{K}(x, x_2) = K_0 + \int_\Gamma H(s, \vec{\xi}) P_\mathrm{x}(x, \xi_2) \mathrm{d}\Gamma \tag{14}$$

with P_x being the bridging force, which can be obtained through[16]

$$0 = V(\vec{x}_\mathrm{x}) + \frac{1-\nu}{\mu} \int_\Gamma M(\vec{x}_\mathrm{x}, \vec{\xi}) P_\mathrm{x}(x, \xi_2) \mathrm{d}\Gamma, \tag{15}$$

where $\vec{x}_\mathrm{x} = (-x, x_2)$ is a point in PGBI. Note that in Eqs. (12)–(15), the origin of the coordinate system is set at the propagating cleavage front.

Substituting Eq. (11) into (10) leads to

$$\frac{a_0}{3} G_\mathrm{cr} - \frac{a_1}{3} G_\mathrm{B} - \frac{1}{w} \int_\Gamma P(\xi_2) V(\vec{\xi}) \mathrm{d}\Gamma = \int_0^{\Delta a} R(x) \mathrm{d}x. \tag{16}$$

Finally, combination of Eqs. (6) and (16) gives the solution of G_cr and Δa as functions of D/w, with D being the width of PGBI (see Fig. 1). Note that Δa depends on the fracture resistance gradient, and thus is different from the crack jump length in an actual bicrystal specimen. In order to solve Eqs. (6) and (16) numerically, an iteration method has been developed. The initial values of $\tilde{G}$ and Δa are obtained by replacing the term of $\int_0^{\Delta a} R(x)\mathrm{d}x$ in Eq. (16) by $G_\mathrm{B}\Delta a$, and then the trial $R(x)$ curve can be obtained through the calculation of the energy release rate at the 10th point from 0 to Δa. For the numerical integration along Γ, the influence of the PGBI more than $5w$ away from the point under consideration is neglected, and $P(\xi_2)$ is taken as a fourth-order polynomial.

Figure 4 shows the numerical results of G_cr. When the size/spacing ratio of PGBI, D/w, is zero, i.e. the PGBI does not exist, $G_\mathrm{cr}/G_\mathrm{B} \to 1$, as it should. As D/w rises, $\tilde{G}$ increases monotonically. When $D/w \to 1$, $\tilde{G} \to \infty$, whereas under this condition due to the pronounced nonlinear interaction between the adjacent PGBI, the numerical process becomes sensitive to the initial condition. According to the experimental observations, in most of the specimens, the D/w ratio is in the range 0.05–0.2, for which the iteration procedure converges quite well.

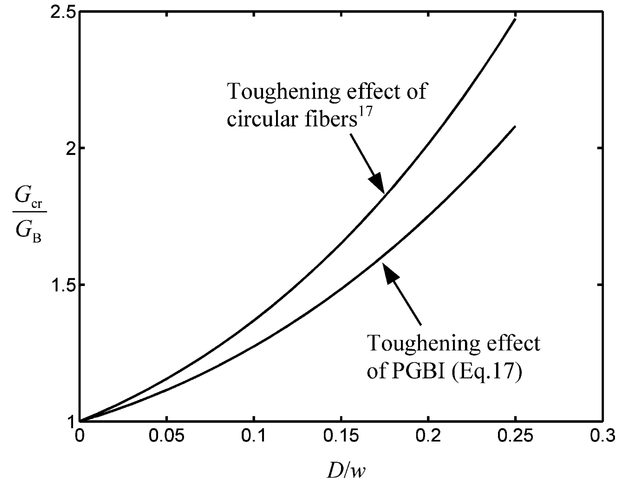

Fig. 4 The relationship between the fracture resistance and the size/spacing ratio of PGBI.

Table 1 Comparison of experimental and theoretical results

Experimental data[13]	θ	0.367	0.332	0.297	0.227
	D/w	0.105	0.080	0.071	0.074
	$\tilde{G}$	1.278	1.208	1.179	1.182
Theoretical result of	$\tilde{G}$ [Eq. (17)]	1.283	1.205	1.170	1.190

In context of line-average theory,[18] the numerical results of the $\tilde{G}$–D/w relation can be regressed as

$$\frac{G_\mathrm{cr}}{G_\mathrm{B}} = \left(1 - \frac{D}{w}\right) + \left(1.7 + 2.4\frac{D}{w} + 0.1\frac{D^2}{w^2}\right)^2 \frac{D}{w}. \tag{17}$$

Compared with the toughening effect of circular fibres with the same size/spacing ratio of reinforcements,[17] which is also shown in Fig. 4, the fracture resistance of high-angle grain boundaries is somewhat less pronounced, primarily due to the high aspect ratio. The experimental and theoretical results are compared in Table 1. The D/w ratio of each sample is taken as the average value of more than 20 PGBI measured from SEM photos.

RESULTS AND DISCUSSION

As discussed above, the bridging force distributed in the PGBI, $P(\xi_2)$, can be obtained by solving the Fredholm integral Eq. (15). When $x = \Delta a$, the resultant force of a PGBI, $\bar{P}$, is calculated and shown in Fig. 5, with $\hat{P} = \frac{\bar{P}}{\tan\theta\left[(w/2)^2(1-D/w)\right]}$ being the average shear stress normalized by the area of triangle PGBI. Because the crack trapping effect is increasingly significant as the area of PGBI rises, $\hat{P}$ increases with the D/w ratio. Note that the effective shear strength of the Fe–3wt%Si alloy, k, was measured to be 144 MPa.[13] Through Eq. (14), it can be seen that $\hat{P}$ is proportional

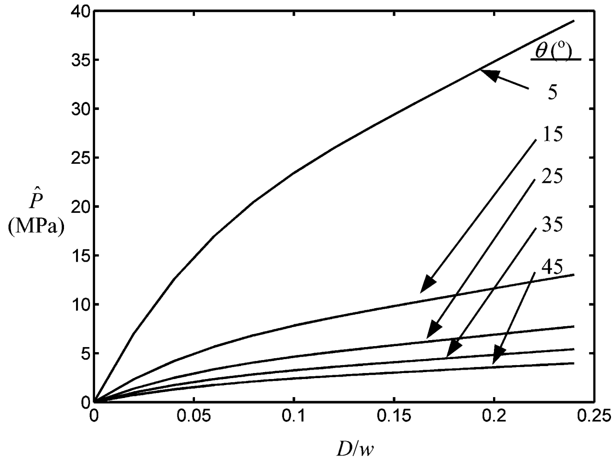

Fig. 5 The bridging force as a function of the *D/w* ratio.

to $\sqrt{G_B}$, and therefore the shear stress tends to increase with θ. When θ rises, on the other hand, the PGBI area becomes larger, which has a beneficial effect to lower the shear stress. Figure 5 indicates that the latter mechanism is more important as $\bar{P}$ decreases with increasing θ. At all the levels of the twist misorientation, the critical D/w ratios above which the shear stress exceeds k is beyond the range under consideration, i.e. the PGBI cannot be separated through plastic shear simultaneously as the crack front breaks through the grain boundary. Thus, the above discussion is self-compatible. If θ is close to zero, because the PGBI area is small, when the D/w ratio exceeds a certain value the PGBI will yield before the crack trapping effect is fully overcome and Eq. (17) can no longer be used. However, under this condition, the barrier effect of grain boundary to cleavage cracking is actually negligible.[12,13]

For a linear elastic material, $\mu = E/2(1+\nu)$. Therefore, the only elastic parameter that can affect the numerical results is Poisson's ratio. According to the numerical results, G_{cr} is insensitive to ν in a broad range from 0.01 to 0.49, indicating that the grain boundary fracture resistance is not directly related to the elastic properties.

Although the above discussion is based on the study of the cleavage cracking behaviour in DCB specimens, the sample geometry does not have influence on the boundary resistance as the geometrical parameters, h and b, vanish in Eqs (6) and (16). Furthermore, the computer simulation shows that G_{cr} is not sensitive to a_0, even though the energy release rate is associated with a. As a_0 changes by a factor of 100, the variation in G_{cr} is smaller than 5%. Therefore, G_{cr} can be considered as a material constant. Note that, although under different loading modes, the crack front–boundary interactions are somewhat different,[19] the effect of fracture mode on G_{cr} is ignored in the current study.

CONCLUSIONS

In a previous experimental study, it was noted that, when a cleavage front encounters a high-angle grain boundary, it firsts penetrates through the boundary at a number of BTPs. Although the separation of the crystallographic planes around the BTPs is quite easy, the failure of the PGBIs between the breakthrough zones demands a significant amount of work associated with plastic shearing and bending. As the bridging stress is below the shear strength, the separation of PGBI cannot occur spontaneously even after the crack trapping effect has been fully overcome. In this article, the crack trapping process is studied in detail through an energy analysis, and the following conclusions are drawn:

1 For high-angle grain boundaries, the PGBI can act as bridging reinforcements.
2 The crack trapping effect of a high-angle grain boundary is predominantly determined by the size/spacing ratio of PGBI. When the D/w ratio is in the range 0.1–0.2, the PGBI causes a 10–30% increase in fracture resistance.
3 The resistance of a grain boundary to cleavage cracking is a material constant, and is determined by G_B and D/w. All the factors come in by affecting these two parameters.

Acknowledgements

Special thanks are due to Professor Ali S. Argon for the valuable suggestions for understanding the experimental results of the Fe–3wt%Si bicrystals.

REFERENCES

1 Hahn, G. T., Averbach, B. L., Owen, W. S. and Cohen, M. (1959) Initiation of cleavage microcracks in polycrystalline iron and steel. In: *Fracture* (Edited by B. L. Averback, D. K. Felbeck, G. T. Jahn and D. A. Thomas). MIT Press, Cambridge, MA, p. 91.
2 Rosenfield, A. R. and Shetty, D. K. (1983) Cleavage fracture of steel in the upper ductile-brittle transition region. *Engng. Fract. Mech.* **17**, 461.
3 Owen, W. S. and Hull, D. (1963) In: *Refractory Metals and Alloys II* (Edited by M. Semchyshen and L. Perlmutter). Interscience, NY.
4 Lin, T., Evans, A. G. and Ritchie, R. O. (1986) A statistical model of brittle fracture by transgranular cleavage. *J. Mech. Phys. Solids* **34**, 477.
5 Knott, J. F. (1997) In: *Cleavage Fracture: George R. Irwin Symposium Proceedings* (Edited by K. S. Chan). TMS, Warrendale, PA, p. 171.
6 Hsia, K. J. and Argon, A. S. (1994) Experimental study of the mechanisms of brittle-to-ductile transition of cleavage fracture in silicon single crystals. *Mater. Sci. Engng.* **A176**, 111.
7 Argon, A. S. and Gally, B. J. (2001) Selection of crack-tip slip systems in the thermal arrest of cleavage cracks in dislocation-free silicon single crystals. *Scr. Mater.* **45**, 1287.

8 Gell, M. and Smith, E. (1967) The propagation of cracks through grain boundaries in polycrystalline 3% silicon iron. *Acta Metall.* **15**, 253.
9 Crocker, A., Smith, G., Flewitt, P. and Moskovic, R. (1996) In: *Proceedings of the 11th European Conference on Fracture (ECF11)*, Vol. 1, *Engng Mater. Advis. Serv.*, Warley, UK, p. 233.
10 Anderson, T. L., Stienstra, D. and Dodds, R. H., Jr. (1994) In: *Fracture Mechanics: Twenty-Fourth Volume*, ASTM STP-1207 (Edited by J. D. Landes, De. E. McCabe and J. A. M. Boulet). ASTM, Philadelphia, PA, p. 186.
11 McClintock, F. A. (1997) A three-dimensional model for polycrystalline cleavage and problems in cleavage after extended plastic flow or cracking. In: *Cleavage Fracture: George R. Irwin Symposium Proceedings* (Edited by K. S. Chan). TMS, Warrendale, PA, p. 81.
12 Argon, A. S. and Qiao, Y. (2002) Resistance of cleavage cracking of high-angle bicrystal grain boundaries in Fe-Si alloy. *Phil. Mag.* **82**, 3333.
13 Qiao, Y. and Argon, A. S. (2003) Cleavage cracking resistance of high angle grain boundaries in Fe-3wt%Si alloy. *Mech. Mater.* **35**, 313.
14 Qiao, Y. and Argon, A. S. (2003) Cleavage crack-growth-resistance of grain boundaries in polycrystalline Fe-2wt%Si alloy: Experiments and modeling. *Mech. Mater.* **35**, 129.
15 Qiao, Y. (2003) Modeling of resistance curve of high-angle grain boundary in Fe-3wt%Si alloy. *Mater. Sci. Engng.* **A361**, 350.
16 Ulfyand, Y. S. (1969) *Survey of Articles on the Application of Integral Transforms in Theory of Elasticity*. University of North Carolina, Raleigh, NC.
17 Qiao, Y., Kong, X. and Pan, E. (2004) Fracture toughness of thermoset composites reinforced by strongly bonded impenetrable short fibers. *Engng Fract. Mech.* **71**, 2621.
18 Rose, L. R. F. (1987) Toughening due to crack front interaction with a 2nd phase dispersion. *Mech. Mater.* **6**, 11.
19 Qiao, Y. and Kong, X. (2004) An energy analysis of the grain boundary behavior in cleavage cracking in Fe-3wt.%Si alloy. *Mater. Lett.* **58**, 3156.